Magnetic ferroelectric metal in bilayer Fe_3GeTe_2 under interlayer sliding

Magnetic ferroelectric metal in bilayer Fe_3GeTe_2 under interlayer sliding

Xiaoyan Miao[1], Milorad Milošević [2], Chunmei Zhang[1,*]
[1]*School of Physics, Northwest University, Xi'an 710127, China*
[2]*Department of Physics, University of Antwerp, Groenenborgerlaan 171, 2020 Antwerp, Belgium*
Email: chunmeizhang@nwu.edu.cn;

The inherent interlayer freedom in van der Waals stacked materials provides an excellent opportunity to investigate ferroelectric-like behavior through interlayer translation. Based on first-principles calculations, we find that the interlayer sliding in Fe_3GeTe_2 (FGT) bilayer enables the coexistence of polarization, metallicity, and ferromagnetism. We find that the polarization is induced by the uncompensated vertical interlayer charge transfer, and can be switched by an in-plane interlayer sliding. A moderate biaxial strain can reverse the polarization direction of the sliding FGT bilayer. The vertical polarization disentangles with the in-plane conductivity as was previously seen in the sliding ferroelectric WTe_2 bilayer. Our work proposes an extremely rare magnetic ferroelectric metal phase that is useful for magnetoelectric and spintronic applications.

Keywords: *Fe_3GeTe_2, ferromagnetic, sliding ferroelectric, polarization, magnetic ferroelectric metal*

1. Introduction

The term 'ferroelectric metal' was introduced by Anderson and Blount in 1965.[1] This pioneering theoretical work first predicted a "ferroelectric" like transition in a metal, which contradicts the traditional belief that the itinerant carriers of a metal would screen the local electric dipole moments between ions, and disfavor polar structure

distortion.[2] Thus, quite a few polar metals have been reported to date. An addition of magnetism produces a "magnetic polar metal", which is an even rare system. This is because the polarization normally originates from the acentric materials with bandgap, while transition-metal *d* orbitals in ferromagnets support centrosymmetric structure. [3-8] Thus, designing or exploring magnetic polar metal phases is challenging. However, a material that integrates magnetic, metallic, and polar behaviors has broad prospects for applications, such as in information storage,[9] unconventional superconductivity,[10] highly anisotropic thermopower,[11] manipulation of magnetic skyrmionics,[12] etc.

It has been evidenced in experiments that metal could afford switchable electric polarization in $LiOsO_3$[13] and WTe_2.[14,15]In addition, magnetic polar metal phases can be designed by heterostructure[16] or doping.[17,18] To seek an ideal magnetic polar metal system with a tunable polarization, we focus on two aspects: (1) a feasible method, and (2) a suitable material. In two-dimensional (2D) van der Waals (vdW) materials, stacking order has been established as often decision for the emergent fundamental properties. The weak interlayer interactions make rotation and translations between layers easy to manipulate, [19,20] and thereby alter the operation of the corresponding physical properties, i.e., the out-of-plane ferroelectricity, [21,22] the ground state magnetism,[23] valley polarization,[24] bulk photovoltaic effect,[25] etc. Recently, the research on interlayer-sliding ferroelectricity, enabling the design of ferroelectric materials out of non-ferroelectric parent compounds, has received great attention because of its accessibility and the possibility to expand to various systems. Achieving out-of-plane polarization reversal through interlayer sliding is also achievable. Experiments have observed such mechanisms in vdW bilayers, multilayers, and even bulk materials. [26-28] Therefore, using interlayer-sliding ferroelectricity to achieve out-of-plane polarization is an ideal method.

Several 2D magnetic materials with long range ferromagnetic (FM) order have been fabricated recently, such as CrI_3,[29] VSe_2,[30] CrSBr,[31] and Fe_3GeTe_2 (FGT).[32] Among them, FGT was the topic of a great number of studies owing to the rare metallic itinerant ferromagnetism [33] down to the monolayer thickness. It exhibits a layered hexagonal centrosymmetric crystal structure with a space group P63/mmc.[34,35] We have recently shown that strain can induce a magnetic polar metal phase in the FGT monolayer.[36]

In this paper, based on first-principal theory calculations, we investigate the possibility of retaining the magnetic polar metal phase in a bilayer FGT, while producing ferroelectricity by sliding one layer with respect to the other. We demonstrate that the vdW stacking modifies both the crystal symmetry and the electronic structure of the FGT bilayer. The most energetically stable sliding operations for FGT bilayer are demonstrated as state-1 (1/3, -1/3) and state-2 (-1/3, 1/3) (direct coordinates relative to lattice). Under these two operations of the relative interlayer sliding translation, the polarization direction of bilayer FGT can be switched due to the interlayer vertical charge transfer. Meanwhile, the interlayer sliding operations (1/3, -1/3) and (-1/3, 1/3) will not affect the ferromagnetic ground state of the FGT system. When electrons are vertically confined, the in-plane conductive electrons are not screened, thus the system still exhibits metallicity. Within a moderate range, an additional compressive strain can change the direction of the emergent polarization, and the magnitude of polarization increases with strain. Overall, we convincingly demonstrate that the interlayer sliding indeed allows for the coexistence of polarization, ferromagnetism, and metallicity in a FGT bilayer.

2. Methods

The density function theory (DFT) calculations are performed using the Vienna ab initio simulation package (VASP).[37,38] The projector-augmented wave (PAW) pseudopotential method[39] and the generalized gradient approximation (GGA) in the Perdew–Burke–Ernzerhof (PBE)[40] form are applied. The DFT-D3 method of Grimme[41] is taken into account to describe the vdW interaction.[42] The plane-wave energy cut-off is set to be 500 eV. The structures are relaxed until the energy and the force on each atom are less than 10^{-6} eV and 0.001 eV/Å, respectively. The Brillouin zone is sampled with a Γ-centered with 8 × 8 × 1 k-mesh for the FGT bilayer. To avoid interlayer interactions between periodic images of the system, the vacuum layer of at least 30 Å is used. The out-of-plane electric polarization of the FGT interlayer sliding is obtained by the classical electrodynamic method. It can be obtained by integrating $\rho \times z$ over the whole supercell, where ρ is the local charge density and z is the coordinate along the out-of-plane c axis.[43,44] The climbing image nudged elastic band method is employed to estimate the ferroelectric switching energy barrier.[45] In this study, dipole

corrections were applied in the calculation of polarization to ensure the accuracy of the results.

3. Results and Discussion

FGT monolayer has been successfully synthesized in experiments.[46,47] In the FGT monolayer, the Fe atoms are located at two inequivalent Wyckoff sites. The FGT monolayer consists of five atomic layers shown in **Figure 1**(a), in which the top and bottom sublayers are comprised of Te atoms (Te_I and $Te_{I'}$ at the equivalent site), while the second and fourth sublayers consist of Fe atoms (Fe_I and $Fe_{I'}$ at the equivalent site). The middle sublayer comprises Fe_{II} and Ge atoms.[48] FGT compound is a layered structure with AB stacking where the two adjacent layers rotate 180° relative to each other. It has inversion symmetry and spontaneously forbids electric dipole moment. If two layers of FGT are parallel stacked, forming AA stacking order, it has vertical symmetry (Mirror z, M_z). However, the state by directly putting two layers together via M_z is unstable, and we denote it as an intermediate (IM) state as shown in Figure 1(a). Two layers would shift relative to each other and polar behavior forms.[25] We consider several possible interlayer sliding patterns, which are shown in Table 1, the interlayer translation operations being (±1/3, 0), (0, ±1/3), (±1/3, ±1/3), and (±1/3, ∓1/3).

Table 1 presents the energy distribution of interlayer sliding along different directions. Through comparing those values, we find that the sliding operations with (1/3, -1/3) and (-1/3, 1/3) are the most energetically stable and are dubbed state-1 and state-2 respectively as shown in Figures 1(b) and 1(c), which is our research focus in the following text. The absolute polarization values for state-1 and state-2 are equal but with opposite directions, $\pm 8.3 \times 10^{-4}$ eÅ/unit cell, respectively, which we denote $P_{\uparrow}$ and $P_{\downarrow}$, respectively. This polarization reversal behavior caused by interlayer sliding can be observed in Figure 1(d). The polarization directions are reversed when the relative sliding between two layers is in opposite directions. The polarization values corresponding to interlayer sliding along the directions of (±1/3, 0) , (0, ±1/3) and (±1/3,±1/3) is $\pm 3.8 \times 10^{-5}$ eÅ/unit cell , $\pm 9.7 \times 10^{-5}$ eÅ/unit cell and $\pm 3.8 \times 10^{-5}$ eÅ/unit cell, respectively. The state-1 and state-2 have the maximum polarization value

and the lowest energy, can be verified in our energy potential diagram shown in Figure S3.

Table 1. Relative energy for bilayer FGT under different sliding operations, with respect to the sliding operations of (1/3, -1/3) and (-1/3, 1/3).

	(1/3,1/3)	(-1/3,1/3)	(1/3,0)	(-1/3,0)	(0, 1/3)	(0,1/3)	(1/3,1/3)	(-1/3,-1/3)
Energy (meV)	0	0	21.4	19.6	20.2	19.8	19.6	19.0

In this work, we focus on the most stable case with controllable polarization value, under interlayer sliding operations (1/3, -1/3) and (-1/3, 1/3). The IM state is nonpolar where the two layers are stacked in parallel. For state-1 as shown in Figure 1(b), the top layer laterally shifts (1/3, -1/3) in fractional coordinates with respect to the bottom layer. This results in a positive dipole moment along the *z* direction, denoted as $P_{\uparrow}$. In contrast, the top layer of state-2 shifts along (1/3, -1/3) relative to the bottom layer, leading to $P_{\downarrow}$ (as shown in Figure 1(c)). The Ge (Fe_{II}) atoms in the top layer sit above the Fe_{II} (Ge) atoms in the bottom layer of state-1 (state-2). Based on the nudge-elastic-band calculation, the switching pathway shown in Figure 1(e) gives an estimation of the energy barrier of 13 meV/unit cell between the $P_{\uparrow}$ and $P_{\downarrow}$ state. Compared with the experimentally accessible systems, this is lower than In_2Se_3 (~ 60 meV/unit cell)[49] and higher than that of WTe_2 (~0.6 meV/unit cell),[14] and verified the possibility of polarization flipping under ambient conditions. The low energy barrier arises from the fact that interlayer sliding to achieve polarization switching only needs to overcome weak interlayer vdW interactions, without involving the deformation of tightly bonded atoms as in the transformation of a bulk ferroelectric.[49]

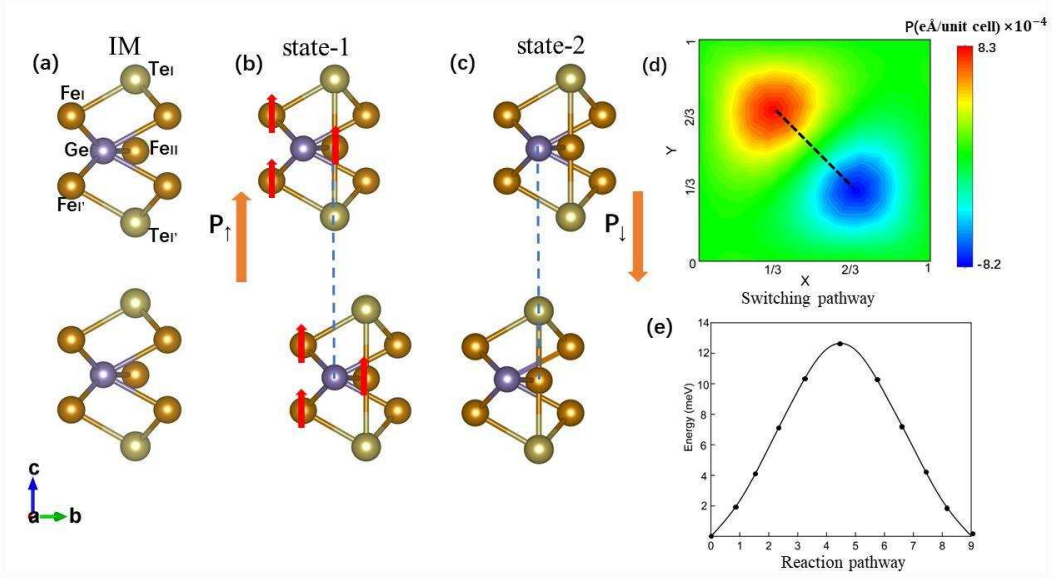

Figure 1. (a-c) Atomic structures of the bilayer FGT for (a) IM, (b) state-1, and (c) state-2. State-1 and state-2 can be obtained by interlayer sliding from IM under sliding operations (1/3, -1/3) ($P_{\uparrow}$) and (-1/3, 1/3) ($P_{\downarrow}$). The orange arrows indicate the polarization direction. The direction of spin is indicated by the red arrows on Fe atoms. (d) Contour plot of vertical polarization versus the sliding direction and distance of the FGT bilayer. A black dotted line indicates the polarization-switching pathway. (e) The energy barrier of the ferroelectric switching pathway from state-1 to state-2.

To explore the origin of vertical polarization, we calculate the charge differences between the top and bottom layers in state-1. As shown in **Figure S1**, we calculate the electron accumulation and dissipation between two individual monolayers of FGT. The reason for the out-of-plane polarization can be revealed by the charge transfer. We use the Bader charge analysis [50] to check the charge gain and loss of the individual layers within bilayer FGT. It is found that the charge gains and losses for the top and bottom layers are 0.03e in state-1. Thus, the two layers are nonequivalent. The charge gains and losses are opposite for state-2. Thus, the polarization can be flipped through the interlayer translation. Here, like the previous works on hBN or MoS_2,[51] the out-of-plane polarization flips with in-plane ion displacements, thus the vertical polarization and interlayer shifting are coupled.

Having confirmed the sliding ferroelectricity in the FGT bilayer, we next investigate the magnetic ground state. We compare the relative values of energy differences between the interlayer FM and antiferromagnetic (AFM) spin configurations as shown in **Table S1**. (we use U* to consider on-site Coulomb

interaction of the Fe 3d orbitals the U* values were computed using a linear response method)[52] The intralayer coupling in FGT is FM.[53] Therefore, for FGT bilayers, we consider the interplay of the intralayer FM and interlayer FM and AFM coupling. Figure 1(b) shows the considered FM configuration, and **Figure S2** shows the AFM counterpart. Table S1 shows the magnetic ground state for each interlayer sliding configuration. As one sees, FM is more energetically favorable compared to AFM for state-1 and state-2, which is we mainly focused on. Compared with bulk FGT, the bilayer is equivalent to the reduction in the number of layers, leading to a reduced Pauli potential for bilayers with respect to thicker layers, increasing the tendency toward FM-type interlayer exchange coupling. The same mechanism explains the reason why the stacking structure of the double layer shows a FM state in this work. Thus, we conduce that the magnetic ground state is unaffected by the sliding operations.

Having confirmed the magnetic ground state of a bilayer FGT, we now focus on its electronic structure. [24,54] **Figures 2**(a) and 2(b) depict the band structures of the monolayer and $P_{\uparrow}/P_{\downarrow}$ of the bilayer FGT system, respectively. As is known, the FGT monolayer exhibits metal ferromagnetism,[55] which can be seen in Figure 2(a). Through comparison between Figures 2(a) and 2(b), we find that the band structures for state-1 and state-2 are different from that of the monolayer. At the same time, from Figure 2(b), we can observe a noticeable difference in the band structures of states-1 and state-2 compared with monolayer FGT. This is because the interlayer sliding breaks the M_z symmetry, and generated out-of-plane dipole moment makes the top and bottom layers inequivalent. [56]

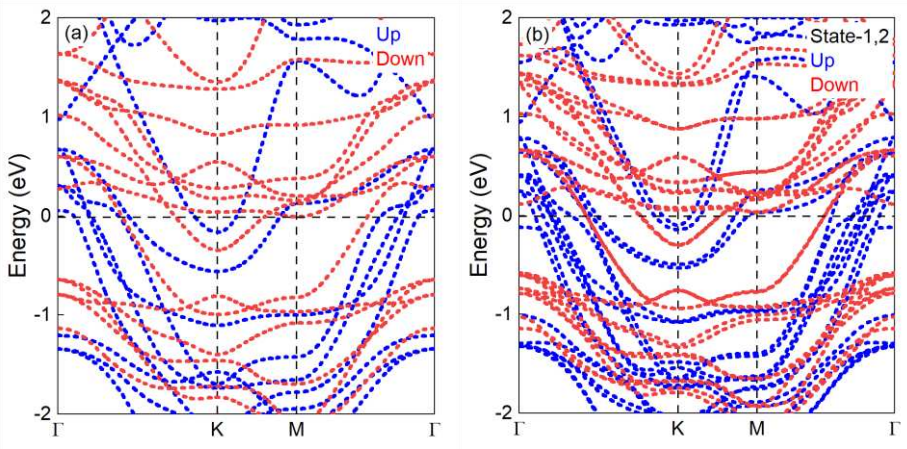

Figure 2. Spin-polarized band structure for (a) FGT monolayer and (b) state-1/state-2 bilayer FGT.

Our work so far has shown that the electric polarization and FM ground state of the bilayer FGT coexist under interlayer sliding. Next, we move on to the discussion of the metallicity. The band structures around the Fermi level are predominantly governed by the Fe 3*d* orbitals.[32] **Figure 3**(a) shows the density of states of the interlayer sliding FGT, confirming that the electronic behavior in the FGT bilayer still arises primarily from the Fe *d* orbitals, maintaining its metallic ground state. Additionally, Figures 3(b) and 3(c) depict the Fe *d* orbitals projected spin-polarized bands in the sliding FGT. These images reveal that the conducting electrons near the Fermi surface predominantly originate from the Fe *d* orbitals. Here, it resembles the experimentally witnessed behavior of a WTe_2 bilayer,[57] where the electrons are vertically confined. The electrons in the plane will not be screened, so the plane still exhibits metallic properties.

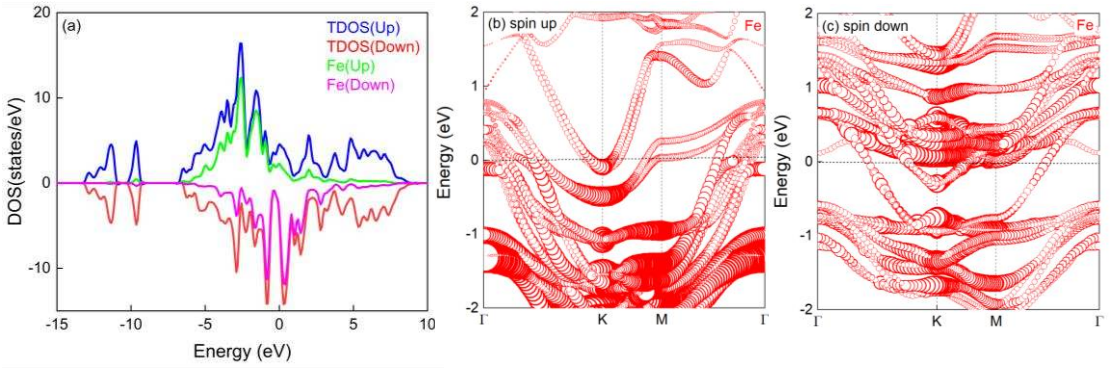

Figure 3. (a) The Fe-*d* orbital projected density of states of state-1 bilayer FGT. Panels (b) and (c) correspond to spin-up and spin-down Fe-*d* orbital-resolved band structure of state-1 and state-2 FGT. The Fermi level is shifted to 0.

Above we successfully demonstrated the switchable polarization in sliding ferroelectricity in FM bilayer FGT. Recently, by applying biaxial strain, significant polarization changes in MnSe bilayers were observed,[58] and the same phenomenon can be observed in FGT monolayers.[36] Therefore, to further modulate the polarization, we discuss the influence of external strain on FGT bilayers. **Figures 4**(a) and 4(b) demonstrate the variation of polarization values of state-1 and state-2 with biaxial compressive strain ε. We can see that strain can change the direction of polarization in our systems, and the polarization value gradually increases with strain. When ε = -1%, -2%, -3%, and -4%, the corresponding polarization values of state-1 are -1.3×10^{-4} eÅ/unit cell, -1.8×10^{-4} eÅ/unit cell, -3.6×10^{-4} eÅ/unit cell and -3.1×10^{-3} eÅ/unit cell, respectively. Likewise, the absolute value of the polarization of state-2 also enhances with strain. To find the mechanism of the strain altering the polarization direction, we further scrutinize the crystalline configuration of the state-1. When external strain is

applied, the structure of state-1 (state-2) is affected. Specifically, in the absence of strain, Fe_{II} and Ge atoms are located at the mirror plane along the z direction of each layer in the bilayer FGT. However, upon the application of strain, the Fe_{II} and Ge atoms deviate from the center and move in opposite directions perpendicular to the plane, upwards and downwards respectively, breaking the vertical symmetry in each layer of the bilayer FGT. As a result, the polarization contribution from both the ionic and electronic parts count, but they have opposite polarization directions. When the polarization contribution from the ionic parts for state-1 (state-2) is more pronounced compared with the electronic part, the polarization direction is reversed.

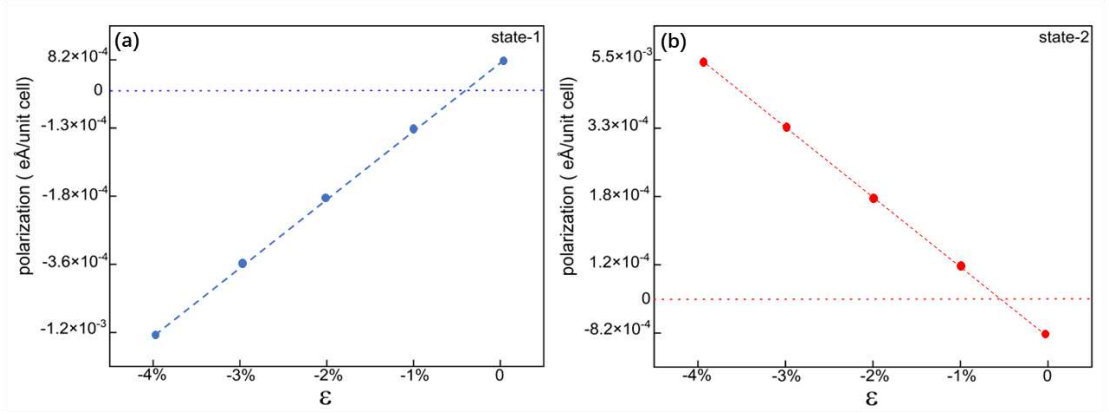

Figure 4. The variation of polarization in (a) state-1 and (b) state-2 bilayer FGT, respectively, as a function of the biaxial in-plane strain.

4. Conclusions

In summary, we demonstrate the coexistence of switchable polarization, ferromagnetism, and metallicity in sliding bilayer FGT. We find that the polarization of the FGT bilayer stems from the uncompensated interlayer vertical charge transfer. In this system the electrons are conducted in-plane and decoupled from the vertical polarization, making bilayer FGT an ideal ferroelectric metal. Further, the interlayer sliding does not alter the metal ferromagnetic ground state, resulting in a rare magnetic ferroelectric metal phase. Furthermore, we reveal that an external strain can change the polarization direction. Our work thus expands the theoretical foundation for creating magnetic metal phases with polar behavior and expands the family of 2D magnetic polar metal materials, which will stimulate further experimental works and practical applications.

Supporting Information

Charge density difference for state-1 upon interlayer sliding. The AFM configuration and the relative energy values for both FM and AFM configurations, the doule well potential diagram for FGT bilayer.

Author information

Chunmei Zhang- *School of Physics, Northwest University, Xi'an 710127, China*

Email: chunmeizhang@nwu.edu.cn

Xiaoyan Miao- *School of Physics, Northwest University, Xi'an 710127, China*

Milorad Milošević- *Department of Physics, University of Antwerp, Groenenborgerlaan 171, 2020 Antwerp, Belgium*

Email：milorad.milosevic@uantwerpen.be

Conflict of Interest

The authors declare no competing financial interest.

Data Availability Statement

The data that support the findings of this study are available from the corresponding author upon reasonable request.

Acknowledgments

We acknowledge the financial support from the National Natural Science Foundation of China (NSFC) under Grant Nos. 12004306, 12274342 and the FWO-FNRS excellence of science project ShapeME. Additionally, the authors acknowledge support from Bianshui Riverside Supercomputing Center (BRSC) and Beijing PARATERA Technology Co., LTD for providing high-performance resources for contributing to the research results reported within this paper.

References

[1] P. W. Aderson, E. I. Blount, *Phys. Rev. Lett.* **1965,** 14, 217-219.
[2] N. A. Hill, *J. Phys. Chem. B* **2000**, 104, 6694-6709.
[3] N. A. Benedek, T. Birol, *J. Mater. Chem. C* **2016,** 4, 4000-4015.
[4] T. H. Kim, D. Puggioni, Y. Yuan, L. Xie, H. Zhou, N. Campbell, P. J. Ryan, Y. Choi,

J. W. Kim, J. R. Patzner, *Nature* **2016,** 533, 68-72.
[5] I. A. Sergienko, V. Sergienko, M. Keppens, R. McGuire, J. Jin, S. He, B. C. Curnoe, P. Sales, D. J. Blaha, K. Singh, *Phys. Rev. Lett.* **2004,** 92, 065501.
[6] T. Kolodiazhnyi, M. Tachibana, H. Kawaji, J. Hwang, E. Takayama-Muromachi, *Phys. Rev. Lett.* **2010,** 104, 147602.
[7] J. Fujioka, A. Doi, D. Okuyama, D. Morikawa, T. Arima, K. N. Okada, Y. Kaneko, T. Fukuda, H. Uchiyama, D. Ishikawa, A. Q. R. Baron, K. Kato, M. Takata, Y. Tokura, *Sci. Rep.* **2015,** 5, 13207.
[8] Y. Shi, Y. Guo, X. Wang, A. J. Princep, D. Khalyavin, P. Manuel, Y. Michiue, A. Sato, K. Tsuda; S. Yu, M. Arai, Y. Shirako, M. Akaogi, N. Wang, K. Yamaura, A. T. Boothroyd, *Nat. Mater.* **2013,** 12, 1024-1027.
[9] W. Eerenstein, N. D. Mathur, J. F. Scott, *Nature* **2006,** 442, 759-765.
[10] S. S. Saxena, P. Monthoux, *Nature* **2004,** 427, 799.
[11] D. Puggioni, J. M. Rondinelli, *Nat. Commun.* **2014,** 5, 3432.
[12] A. Fert, N. Reyren, V. Cros, *Nat. Rev. Mater.* **2017,** 2, 17031.
[13] J.-G. Cheng, J.-S. Zhou Y. Uwatoko, *ECS J. Solid State Sci. Technol.* **2022,** 11, 023008.
[14] Q. Yang, M. Wu, J. Li, *J. Phys. Chem. Lett.* **2018,** 9, 7160-7164.
[15] X. Liu, Y. Yang,T. Hu, G. Zhao, C. Chen,; W. Ren, *Nanoscale* **2019,** 11 18575-18581.
[16] M. Shen, Y. Weng, Y. Yi, Q. Geng, W. Yan, H. Wang, J. Yang, X. Li, *J. Appl. Phys.* **2019,** 126, 085307.
[17] R. Du, Y. Wang, M. Cheng, P. Wang, H. Li,W. Feng, L. Song, J. Shi, J. He, *Nat. Commun.* **2022,** 13, 6130.
[18] T. Xu, J. Zhang, Y. Zhu, J. Wang, T. Shimada, T. Kitamura, T. Zhang, *Nanoscale Horiz.* **2020,** 5, 1400-1406.
[19] A. K. Geim, I. V. Grigorieva, *Nature* **2013,** 499, 419-425.
[20] K. S. Novoselov, A. Mishchenko, A. Carvalho, A. H. Castro, *Science* **2016,** 353, aac9439.
[21] J. Xiao, Y. Wang, H. Wang, C. D. Pemmaraju, S. Wang, P. Muscher, E. J. Sie, C. M. Nyby, T. P. Devereaux, X. Qian, X. Zhang, A. M. Lindenberg, *Nat. Phys.* **2020,** 16, 1028-1034.
[22] P. Sharma, F. Xiang, D. Shao, D. Zhang, E. Y. Tsymbal, A. R. Hamilton, J. Seidel, *Sci. Adv.* **2019,** 5, eaax5080.
[23] W. Chen, Z. Sun, Z. Wang, L. Gu, X. Xu, S. Wu, C. Gao, *Science* **2019,** 366(6468), 983-987.
[24] T. Zhang, X. Xu, B. Huang, Y. Dai, Y. Ma, *NPJ Comput. Mater.* **2022,** 8, 64.
[25] C. Zhang, P. Guo, J. Zhou, *Nano Lett.* **2022,** *22*(23), 9297-9305.
[26] T. Zhong, M. Wu, *Acta. Phys. Sin.* **2020,** 69, 217707.
[27] C. L. Freeman, F. Claeyssens, N. L. Allan, J. H. Harding, *Phys. Rev. Lett.* **2006,** 96, 066102.
[28] K. Yasuda, X. Wang, K. Watanabe, T. Taniguchi,; H. Jarillo, T. A. Palomaki, *Science* **2021,** 372, 1458–1462.
[29] B. Huang, G. Clark, N. Moratalla, D. R. Klein, R. Cheng, K. L. Seyler, D. Zhong,

E. Schmidgall, M. A. McGuire, D. H. Cobden, *Nature* **2017,** 546, 270-273.
[30] M. Bonilla, S. Kolekar, Y. Ma, H. C. Diaz, V. Kalappattil, R. Das, T. Eggers, H. R. Gutierrez, M. H. Phan, M. Batzill, *Nat. Nanotechnol* **2018,** 13 289-293.
[31] K. Lee, A. H. Dismukes, E. J. Telford, R. A. Wiscons, J. Wang, X. Xu, C. Nuckolls, C. R. Dean, X. Roy, X. Zhu, *Nano. Lett.* **2021,** 21, 3511-3517.
[32] H. Zhuang, K, P. R. Cent, R. G. Hennig, *Phys. Rev. B* **2016,** 93,134407
[33] X. Chen, Z. Lin, L. Cheng, *Chin. Phys. B* **2021,** 30, 047502.
[34] J. Xu, S.Wang, W. Wang, Y. Zhou, X. Chen, Z. Yang, Z. Qu, *Chinese Phys. Lett.* **2020,** 37, 076202.
[35] I. K. Park, C. Gong, K. Kim, G. Lee, *Phys. Rev. B* **2022,** 105, 014406.
[36] X. Miao, S. Li, Z. Jiang, C. Zhang, A. Du, *Phys. Chem. Chem. Phys.* **2023,** 25, 18826-18832.
[37] G. Kresse, J. Furthmüller, *Comput. Mater. Sci.* **1996,** 6(1), 15−50.
[38] G. Kresse, J. Furthmüller, *Phys. Rev. B* **1996,** 54, 11169−11186.
[39] P. E. Blochl, *Phys. Rev. B* **1994,** 50, 17953-17979.
[40] J. P. Perdew, K. Burk, M. Ernzerhof, *Phys. Rev. Lett.* **1996,** 77 (18), 3865−3868.
[41] S. Grimme, J. Antony, S. Ehrlich, H. Krieg, *J. Chem.Phys.* **2010,** 132, 154104.
[42] J. Klimeš, D. R. Bowler, A. Michaelides, *Phys. Rev. B* **2011,** 83, 195131.
[43] C. Zhang, L. Zhang, C. Tang, S. Sanvito, B. Zhou, Z. Jiang, A. Du, *Phys. Rev. B* **2020,** 102,134416.
[44] W. Ding, J. Zhu, Z. Wang, Y. Gao, D. Xiao, Y. Gu, Z. Zhang, W. Zhu, *Nat. Commun.* **2017,** 8, 14956.
[45] H. Henkelman, B. P. Uberuaga, H. Josson, *J. Chem. Phys.* **2000,** 113, 9901–9904
[46] Y. Deng, Y. Yu, Y. Song, J. Zhang, N. Wang, Z. Sun, Y. Yi, Y. Wu, S. Wu, J. Zhu, J. Wang, X. Chen, Y, Zhang, Nature 2018, 563, 94–99
[47] A. F. May, S. Calder, C. Cantoni, H. Cao, M. A. McGuire, *Phys. Rev. B* **2016**, 93, 014411.
[48] X. Chen, Z. Lin, L. Cheng, *Chinese Phys. B* **2021,** 30, 047502.
[49] W. Ding, J. Zhu, Z. Wang, Y. Gao, D. Xiao, Y. Gu, Z. Zhang, W. Zhu, *Nat. Commun.* **2017,** 8, 14956.
[50] G. Schaftenaar, J. H. Noordik, *J Compute Aided Mol. Des.* **2000,** 14(3), 233-242.
[51] L. Li, M. Wu, *ACS Nano,* **2017,** 11, 6382-6388.
[52] S. de Gironcoli, M. Cococcioni, Phys. Rev. B **2005**, 71, 35105.
[53] S. Jang, H. Yoon, M. Y. Jeong, S. Ryee, H, S. Kim, M. J. Han, *Nanoscale* **2020,** 12 13501-13506.
[54] K. F. Mak, C. Lee, J. Hone, J. Shan, T. F. Heinz, *Phys. Rev. Lett.* **2010,** 105, 136805.
[55] Y. Wang, C. Xian, J. Wang, B. Liu, L. Ling, L. Zhang, L. Cao, Z. Qu, Y. Xiong, *Phys. Rev. B* **2017,** 96, 134428.
[56] C. Zhang, Y. Nie, S. Sanvito, A. Du, *Nano. Lett.* **2019,** 19, 1366-1370.
[57] Z. Fei, W. Zhao, T. A. Palomaki, B. Sun, M. K. Miller, Z. Zhao, J. Yan, X. Xu, D. H. Cobden, *Nature* **2018,** 560, 336-339.
[58] K. Liu, X. Ma, S. Xu, Y. Li, M. Zhao, *NPJ Comput. Mater.* **2023,** 9, 16.